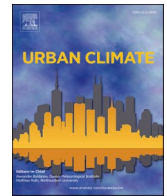




ELSEVIER

Contents lists available at ScienceDirect

Urban Climate

journal homepage: www.elsevier.com/locate/uclim

Trends in synoptic heat events in four Minnesota urban areas through the 21st century

Jonathan F.H. Birkel^a, Tracy E. Twine^{a,*}, Stefan Liess^a, Larry S. Kalkstein^b, Scott Sheridan^c

^a Department of Soil, Water, and Climate, University of Minnesota-Twin Cities, 439 Borlaug Hall, 1991 Upper Buford Ave, St Paul, MN 55108, USA

^b Applied Climatologists, 896 Banyan Court, Marco Island, FL 34145, USA

^c Department of Geography, Kent State University, Kent, OH, 44242, USA

ARTICLE INFO

Keywords:

United States
Spatial synoptic classification
Heat
Excess heat factor
CMIP5
Climate change

ABSTRACT

Extreme heat is often overlooked as a public health concern in Minnesota, where intraseasonal summer variability limits acclimatization to oppressive heat conditions. Specific categories of synoptic-scale air masses are linked to summer excess mortality and elevated health risk in the Midwestern United States, particularly within urban areas. Between 1948 and 2019, Minnesota's four largest urban areas have experienced decreased nighttime cooling, while warmer and more humid air masses have increased in frequency at the expense of cooler and drier ones. We used downscaled CMIP5 climate projections for 21st-century Minnesota, under RCP4.5 and RCP8.5 emissions scenarios, to generate daily synoptic classifications and evaluate projected frequency and character trends in the highest-risk air masses. Projections show dramatic increases in both the frequency and temperature of days within the Dry Tropical category, neither of which have changed significantly thus far across Minnesota's historical record. Frequency and duration of consecutive-day episodes of excess heat, as identified either by synoptic classifications or by the Excess Heat Factor, are likewise expected to increase more substantially in the future than they have in the past. Other projected trends, such as rising dew point temperatures and nighttime air temperatures, represent continuations of already existing historical trends.

1. Introduction

Extreme heat is the leading weather-related cause of human mortality in the United States, exceeding the combined annual mortality rates from other causes such as hurricanes, lightning, tornadoes, and floods (Lee, 2013; Luber and McGeehin, 2008); however, public perception tends to underestimate the risks associated with extreme heat events due to the lack of physical destruction they leave behind compared to other extreme weather events (Luber and McGeehin, 2008). During extreme heat events, increases in hospital admissions often extend well beyond the mortality response, as observed in the Chicago heatwave of July 1995, in which over 700 deaths and over 1000 excess hospital admissions occurred (Semenza et al., 1999).

There is a gap in our understanding of how cities in northern climates will respond to projected increases in heat events. Most

* Corresponding author at: Department of Soil, Water, and Climate, University of Minnesota-Twin Cities, 439 Borlaug Hall, 1991 Upper Buford Ave, St Paul, MN 55108, USA.

E-mail addresses: birkel11@umn.edu (J.F.H. Birkel), twine@umn.edu (T.E. Twine), liess@umn.edu (S. Liess), larryk@miami.edu (L.S. Kalkstein), ssherid1@kent.edu (S. Sheridan).

<https://doi.org/10.1016/j.uclim.2022.101307>

Received 28 March 2022; Received in revised form 16 September 2022; Accepted 21 September 2022

Available online 5 October 2022

2212-0955/© 2022 The Authors. Published by Elsevier B.V. This is an open access article under the CC BY-NC-ND license (<http://creativecommons.org/licenses/by-nc-nd/4.0/>).

analyses of synoptic characteristics related to heat have been in cities where heat events are more prevalent or where rare but strong heat events have already raised awareness in the public, such as in Chicago (Hondula et al., 2014). In contrast, heat events in the Minneapolis-St Paul metropolitan region that are less frequent but expected to increase in the future (Vose et al., 2017; Liess et al., 2022) would reach a less prepared population. Given the location of this region between the more humid east and more arid west, it is unknown whether increases in heat events will be a result of warm, dry air masses or warm, humid air masses—and this difference in humidity has important implications for heat stress.

Every location has a unique set of sensitivities in the connections between heat and mortality, and several studies have generated predictive algorithms for specific cities or regions (Hayhoe et al., 2010; Sheridan and Kalkstein, 2004). Due to the human body's ability to adjust to heat, the same high temperature conditions will have a lesser impact in a more consistently hot location, such as Arizona, than in a colder or less consistently hot location like Minnesota (Folkerts et al., 2020). Furthermore, a hot day late in a summer season will present less danger than an equally hot day in early summer in the same location due to seasonal acclimatization (Nairn and Fawcett, 2014; Sheridan et al., 2009). The severity of a heat event is also influenced by the diurnal temperature range, since nighttime cooling can provide relief from a day of excessive heat, and therefore a warmer night following a hot day can exacerbate its adverse health impacts (Vanos et al., 2014). Likewise, days of excess heat are typically most harmful when they occur consecutively; the impacts of heat upon health are cumulative as heat loads build up (Nairn and Fawcett, 2014).

The U.S. Midwest has a particularly strong sensitivity in heat-health relationships due to the high intraseasonal variability of its regional climate, with both tropical and polar synoptic weather regimes exerting a substantial influence throughout most of the seasonal cycle (Kalkstein and Davis, 1989; Sheridan et al., 2009; Sheridan and Dixon, 2017). Relationships between mortality and temperature alone have been recognized to be non-linear, particularly in the most extreme cases where multiple risk factors compound to produce a deadlier situation (Anderson and Bell, 2009). Therefore, the identification of “weather situations,” based on an ensemble of weather elements, can often delineate the potential for heat-stress conditions more successfully. The Spatial Synoptic Classification (SSC) employs a range of single-station surface observations to evaluate synoptic-scale atmospheric circulation patterns (Sheridan, 2002). The SSC then categorizes daily weather conditions under a series of synoptic air mass types, applying location-specific climatological thresholds that shift with the seasonal cycle. This system enables patterns of adverse health outcomes to be tied to atmospheric circulation behaviors, in which specific synoptic categories or subcategories may be associated with above-baseline mortality responses. Applications of the SSC to weather forecasts can therefore aid in predicting and issuing warnings for health-threatening weather conditions (Hondula et al., 2014; Kalkstein et al., 2011; Sheridan and Kalkstein, 2004). A key advantage of the SSC is its ability to highlight non-uniformities within a changing climate, such as if temperature or other meteorological character changes are concentrated within a certain subset of air mass types rather than being evenly distributed across all days.

While heatwaves are driven by synoptic-scale processes, the urban heat island effect can amplify their impacts locally beyond those received by surrounding rural areas (Fischer et al., 2012; Founda and Santamouris, 2017; Habeeb et al., 2015). Unequal access to air conditioning is also a critical underlying factor in relative risk of heat-related mortality, along with neighborhood disparities in tree cover and quality of construction materials (Harlan et al., 2006).

Many studies have projected the frequency, severity, and duration of extreme heat events in the U.S. to increase throughout the 21st century (Dahl et al., 2019; Hayhoe et al., 2010; Kalkstein and Greene, 1997; Lau and Nath, 2012; Meehl and Tebaldi, 2004). Heat events of comparable severity to the historically unprecedented Chicago heatwave of 1995 may impact the Midwest every other year by end-century even if carbon emissions are substantially reduced, or up to three times a year if emissions remain high (Hayhoe et al., 2010). Meanwhile, heat events exceeding historical precedent are expected to become more commonplace, most concentrated in the Midwest, Southeast, and Southern Plains (Dahl et al., 2019; Lau and Nath, 2012). Though the impacts of heat upon health are widely expected to increase in severity due to climate change, such impacts are already observable: over a third of summer-season heat-related deaths that occurred globally between 1991 and 2018 can be attributed to anthropogenic climate change (Vicedo-Cabrera et al., 2021).

Specifically within Minnesota, observed warming trends are strongest in winter, and this is expected to remain the case throughout the 21st century. However, Minnesota's summers are projected to warm up to 4 °C by the end of the century, with the greatest temperature increases occurring in the northern and central regions of the state (Liess et al., 2022). In light of these climate forecasts, and given Minnesota's susceptibility to heat-related health risks, we aim to evaluate trends in health-threatening heat conditions in four of Minnesota's urban regions. In examining historical synoptic trends, we partially follow the analyses of Midwestern urban centers performed by Vanos et al. (2014), with inclusion of additional urban locations and neighboring rural locations, and under an updated version of the SSC. Utilizing newly available dynamically-downscaled climate projections (Liess et al., 2022), we examine the continuation of such trends into the middle and late 21st century and additionally evaluate a separate temperature anomaly-based metric for excess heat. Rather than simply analyze the Liess et al. dataset, our approach makes use of the SSC to discretize variables into air mass categories, and thus provide a practical way for risk managers and other people to plan for changes in potentially harmful weather events in Minnesota cities. We demonstrate a method, and produce a dataset, that can be used with similar analyses of other urban areas to not only compare and contrast changes in variables such as temperature, but in synoptic character of heat events projected through the 21st century, particularly in regions that have so far seen limited impacts of heatwaves.

2. Material and methods

2.1. Station observations

Historical temperature records were downloaded from the airport weather stations in Minneapolis-St. Paul, Rochester, Duluth, and Fargo-Moorhead from the Midwest Regional Climate Center (MRCC) cli-MATE Online Data Portal (<http://mrcc.purdue.edu>). These

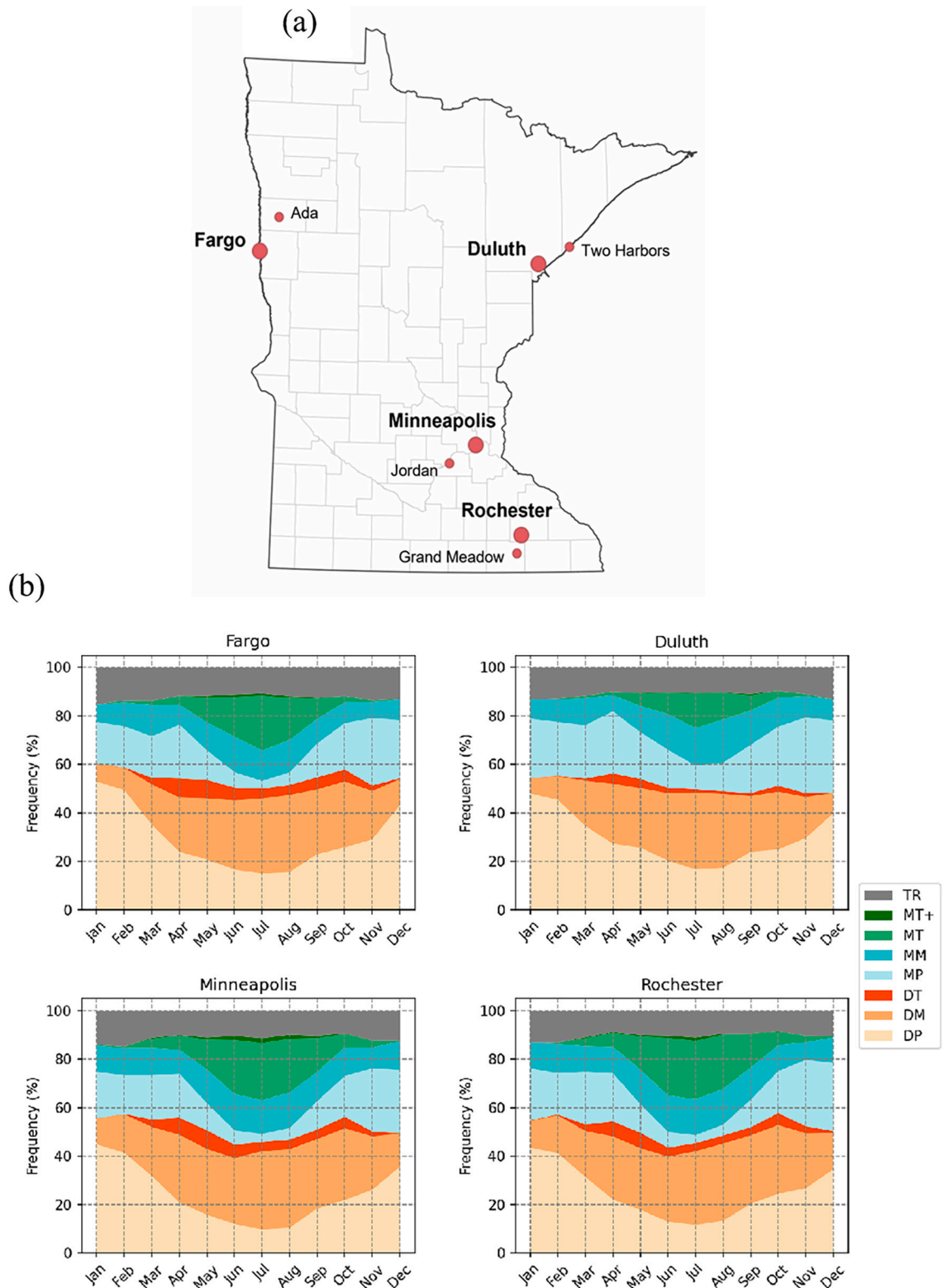


Fig. 1. (a) Locations of weather stations from which historical temperature records were used. Larger markers labeled in bold represent urban airport stations. (b) Monthly frequency (percent of total days in each month) of air mass types by location, averaged over 1948–2019, where the air mass types are defined as transitions between a single air mass (TR), strong moist tropical (MT+), moist tropical (MT), moist moderate (MM), moist polar (MP), dry tropical (DT), dry moderate (DM), and dry polar (DP).

represent the four largest metropolitan areas in or partially in Minnesota for which SSC calendars are available and also represent spatial variability across Minnesota's climate (Fig. 1a). All four stations are within warm or hot summer humid continental Köppen climate regions, with an average annual precipitation gradient from Fargo-Moorhead (M:35 °C, N:-31 °C) of 610 mm, to Duluth (M:32 °C, N:-31 °C) and Minneapolis-St. Paul (M:35 °C, N:-27 °C) of about 800 mm, to Rochester (M:34 °C, N:-29 °C) of 890 mm, according to NOWdata from <http://weather.gov> for 1991–2000 where M (N) is the mean annual extreme maximum (minimum) air temperature. Fargo-Moorhead is located in a flat river valley, Duluth is located on the western shore of Lake Superior, Rochester is located along a river with gentle hills, and the Minneapolis-St Paul region comprises two major rivers and several lakes. Weather stations in Jordan, Grand Meadow, Two Harbors, and Ada were paired with these four urban sites, respectively, in an attempt to capture urban-rural distinctions in air mass character. These sites were selected to be fairly near (35–55 km) their respective urban sites, while covering an equivalent period of record. Thus, rural sites would be presumably close enough to experience the same daily synoptic conditions as their urban counterparts, while simultaneously far enough to avoid any potential urban heat island (UHI) influence. Worth noting, however, are the distinctions in how each airport station is situated relative to its respective urban area. The MSP airport lies within the Minneapolis-St. Paul metropolitan area, aligned with its innermost suburban ring, and has been recognized for the strength of its UHI signal relative to other metropolitan locations outside of the downtown areas of Minneapolis and St. Paul (Smoliak et al., 2015). The other three airports lie outside or along the edges of their respective urban environments, none of which are as physically expansive as Minneapolis-St. Paul. These urban stations may therefore experience less pronounced urban heat island effects.

Daily minimum and maximum air temperatures were available from 1948 to 2019 in all eight locations, while hourly air temperatures and dew point temperatures were only available from the four urban locations. Therefore, for consistency, daily minima and maxima were used in all urban-rural air mass character comparisons. In urban-only synoptic evaluations, consistent 12-h-interval observations from 3:00 and 15:00 Central Standard Time were applied instead, with the temperature difference between these times functioning as an alternate expression of diurnal temperature range. The use of 12-h synoptic observations offers more specific insight into the behavior of the diurnal cycle under different air mass types than a reliance on an assumption of minimum temperatures occurring at night or early morning. Given the physiological relief from hot days provided specifically by cool nights, this distinction has important implications for health (Vanos et al., 2014).

2.2. Observed synoptic classifications

The Spatial Synoptic Classification (SSC) categorizes weather situations under a series of air mass types, incorporating surface observations of air temperature, dew point temperature, cloud cover, wind speed and direction, and pressure at six-hour intervals to provide a holistic representation of daily atmospheric conditions over a location (Kalkstein and Greene, 1997; Sheridan, 2002). The SSC features seven main air mass categories: Dry Polar (DP), Dry Moderate (DM), Dry Tropical (DT), Moist Polar (MP), Moist Moderate (MM), Moist Tropical (MT), and transition days (TR). These categories serve as an extension from the four traditional Bergeron (1930) air mass categories (cP, cT, mP, mT), providing more versatility for health-related and other climatological studies, with greater representation of the modifications that air masses can undergo as they advect over land or water surfaces outside their source regions (Sheridan, 2002). The most recent version of the SSC algorithm (i.e., SSC3; <http://sheridan.geog.kent.edu/ssc3.html>) includes a subtype of each classification to denote more extreme conditions. For example, MT+ is used to classify days on which apparent temperatures exceed the local MT seed-day mean by at least one standard deviation (Sheridan et al., 2009). Air masses are classified daily for a given location through the use of seed days, which exemplify typical weather conditions that each air mass type would bring to that location at a given time of season—a climatological norm—based on the 1981–2010 period.

Most health-related studies focus on the DT and MT+ categories as they represent the hottest summer weather conditions occurring at a given location, distinguished from each other by the relative presence or absence of humidity (L. S. Kalkstein and Greene, 1997; Sheridan and Kalkstein, 2004; Vanos et al., 2014). Due to their lower dew points, and therefore lower cloud cover and specific heat, DT air masses are typically able to reach the highest temperatures of any synoptic type, while facilitating a wider diurnal range than MT or MT+ air masses. Although the designation of MT+ and DT as oppressive types is not universal, the use of MT+ and DT in representing higher-risk conditions is well-established in synoptic heat-health studies of the Midwest (Hayhoe et al., 2010; L. S. Kalkstein and Greene, 1997; Sheridan et al., 2009; Vanos et al., 2014) and is therefore applied here. Daily SSC calendars were downloaded for 1948–2019 from <http://sheridan.geog.kent.edu/ssc3.html> for the four urban airport stations. For purposes of this analysis, all “plus” types were aggregated with their parent types except for MT+, due to its distinct significance from MT in heat-health studies. Rare cases of even more extreme MT++ days were likewise aggregated with MT+.

2.3. Simulated synoptic classifications

We used the SSC algorithm to classify synoptic conditions for both historic and future time periods to evaluate whether projected changes to Minneapolis-St Paul climate can be linked to changes in the occurrences of DT and MT air masses. Liess et al. (2022) used the Weather Research and Forecast (WRF) model to dynamically downscale eight general circulation models (GCMs) to a 10 km horizontal resolution over Minnesota. WRF output data were provided for two emissions scenarios, RCP4.5 and RCP8.5, and for three time periods: 1980–1999, 2040–2059, and 2080–2099. These scenarios are referred to as HIST, MID, END4.5, and END8.5. Only the RCP4.5 results are given for MID as the RCP4.5 and RCP8.5 scenarios diverged mostly by the end of the 21st century. Linear-scaling bias adjustments were applied to temperature and precipitation output with gridded climate normals from PRISM Climate Group (Daly et al., 2017; Liess et al., 2022). Other meteorological output was not bias-adjusted due to the limited availability of observational data.

WRF data were analyzed from a single grid cell that was selected to represent the location of the Minneapolis-St Paul International airport station (Fig. S1). Given the coarseness of the 10 km spatial resolution remaining after downscaling, no attempt was made to distinguish between urban and rural areas. Representation of land cover is limited in both the WRF and GCM simulations, and it is outside the scope of this work to simulate future urban growth and development that might influence land-air interactions.

Required inputs for the SSC algorithm were generated using simulated air temperature, dew point temperature, and horizontal wind vectors at 6-h intervals (3:00, 9:00, 15:00, and 21:00 in local Central Standard Time). A simple linear function of simulated daily mean air temperature along with climatological mean values downloaded from MRCC (<http://mrcc.purdue.edu>) were used to produce daily sea level pressure values. Daily values of cloud cover were estimated from simulated incoming shortwave radiation. Wind direction was unavailable from the downscaled outputs of the bcc-csm1-1 and MIROC5 GCMs, as well as CNRM-CM5 in the END8.5 scenario. The primary consequence of these data constraints was that the lack of pressure variability within each day, as well as the lack of shifts in wind direction under some GCM-scenario combinations prevented synoptic transitions from being accurately calculated in the algorithm. As a result, the TR category was removed from the list of possible synoptic categories and every day that would have been designated as TR was instead assigned the next closest fitting air mass type.

Eight 20-year SSC calendars were produced for each climate scenario—each one derived from a different downscaled GCM resulting in 160 model-years per scenario. We also produced a single 20-year SSC calendar from the average of all downscaled GCMs; however, this overly moderated the meteorological variability relative to observations and resulted in an overrepresentation of moderate synoptic types like DM and near-exclusion of rarer and more extreme types like MT+.

2.4. Air mass trends

We focus our analysis on four types of SSCs: DP, DT, MT, and MT+. While DT and MT+ are generally the most oppressive and health-threatening types in the Midwest, MT is also sometimes associated with above-baseline summer mortality and morbidity. DP days may provide cooling relief in Midwestern summers (Vanos et al., 2014), and we wanted to evaluate whether MSP might see fewer DP days in future summers. Here we define the summer season as May 20 to September 10 to accommodate the potentially expanding seasonal spread of oppressive conditions under climate change.

2.5. The Nairn-Fawcett excess heat factor

There is no universal standard for defining heatwaves and many location-specific heatwave metrics exist (Habeeb et al., 2015; Nairn and Fawcett, 2014; Sheridan and Dixon, 2017; Watts and Kalkstein, 2004). These may capture different events consequential to health that might not be fully captured by MT+ or DT air mass classifications. For example, the well-documented Chicago heatwave of July 1995 (Hayhoe et al., 2010; Meehl and Tebaldi, 2004) peaked under DT and MT+ conditions from July 12–15, but was extended by additional MT days on July 11, 16, and 17.

We classified heatwave days according to the Excess Heat Factor (EHF) of Nairn and Fawcett (2014). The EHF identifies heat events that pose a significant risk to health, reflecting location-specific climatological norms, cumulative impacts of heat, influences of nighttime alongside daytime temperatures, and the effects of acclimatization. Since its introduction, further studies have evaluated its performance in predicting health outcomes, with promising results in Australia and elsewhere (Loridan et al., 2016; Nairn et al., 2018; Scalley et al., 2015). A positive EHF value indicates that the average daily mean temperature (DMT) exceeds the 95th-percentile DMT for a given location (T_{95}). The magnitude of this exceedance of T_{95} (significance index, or EHI_{sig}) is then multiplied by the exceedance of the previous thirty days' average DMT to represent acclimatization (acclimatization index, or EHI_{accl}). Early-season heat events tend to exceed their preceding weeks' temperatures by greater margins than late-season heat events, and thus often result in the greatest excess mortality outcomes (Nairn and Fawcett, 2014; Sheridan et al., 2009). Any day within a three-day period flagged as a heat event is counted as a heatwave day even if its individual DMT does not exceed T_{95} . Conversely, a day whose DMT exceeds T_{95} is not counted if it does not fall within a positive-EHF three-day period. The same qualifications apply to severe heatwave days, or days within three-day periods whose EHF exceeds the 85th-percentile EHF value.

Nairn and Fawcett (2014) define DMT as the average of daily maximum and daily minimum temperature. In order to reflect the distinct health impacts of a hot night following a hot day, maximum and minimum temperatures are selected within 24-h periods beginning and ending at 9:00 rather than midnight, in accordance with Australian weather data formatting conventions. In this analysis, DMT was defined as the average of 12-h temperatures at 15:00 and the following 3:00. This follows the air mass temperature trend analyses outlined above, but reconfigured so that nighttime temperatures follow daytime temperatures rather than aggregating times by calendar date.

Length of heatwave season was defined as the duration from each year's first heatwave day to its last (Habeeb et al., 2015). For each year, heatwave intensity was expressed as the mean exceedance of T_{95} on heatwave days. Heatwave duration was defined as the average number of heatwave days occurring consecutively per heat event, regardless of whether all of them exceed T_{95} individually, while heatwave frequency was defined as the number of these events per year.

Table 1

Summary statistics for urban sites' air mass frequency (days per season), air temperature (Ta; °C), and dew point temperature (Td; °C) trends over 1948–2019 within the May 20–September 10 season. Linear regression slopes are expressed as decadal rather than yearly changes. Bold slope and R2 values indicate $p < 0.05$ significance.

		All			DP			DT			MT			MT+		
		Mean	Slope	R ²	Mean	Slope	R ²	Mean	Slope	R ²	Mean	Slope	R ²	Mean	Slope	R ²
Minneapolis	Frequency	–	–	–	11.1	–1.079	0.134	6	0.164	0.003	26.1	1.691	0.163	2	0.152	0.023
	3:00 T _a	17.3	0.297	0.270	12.1	0.178	0.065	20.1	0.12	0.01	20	0.167	0.144	24.3	0.085	0.012
	3:00 T _d	13.6	0.184	0.121	8.5	0.046	0.004	14.1	–0.005	0	16.9	0.099	0.060	18.9	0.117	0.016
	15:00 T _a	25.4	0.055	0.009	21.2	–0.043	0.007	32.3	–0.195	0.048	28.2	–0.046	0.017	33.1	–0.073	0.013
	15:00 T _d	13.8	0.097	0.03	8	–0.097	0.015	13.7	–0.392	0.055	18.1	–0.023	0.002	19.9	–0.117	0.018
Rochester	Frequency	–	–	–	13.5	–0.01	0	4.6	–0.529	0.035	27	1.801	0.152	1	0.061	0.007
	3:00 T _a	15.6	0.143	0.092	10.6	0.192	0.112	17.8	–0.054	0.002	18.8	0.013	0.001	23.4	–0.053	0.006
	3:00 T _d	13.2	0.211	0.145	8.3	0.173	0.070	13.1	–0.175	0.011	16.8	0.106	0.065	19.7	0.077	0.009
	15:00 T _a	24.4	–0.082	0.02	20.7	–0.016	0.001	31.2	–0.102	0.012	27.4	–0.139	0.141	32.6	–0.08	0.014
	15:00 T _d	14.6	0.257	0.179	9.2	0.282	0.116	13.7	–0.413	0.061	18.9	0.14	0.100	20.9	0.013	0
Duluth	Frequency	–	–	–	19.8	–1.128	0.109	2.2	–0.017	0	12.8	1.188	0.145	0.3	0.021	0.005
	3:00 T _a	12.8	0.259	0.250	8.5	0.223	0.187	15.9	–0.119	0.008	17.5	0.081	0.022	21.4	–0.269	0.068
	3:00 T _d	10.2	0.196	0.124	6	0.141	0.050	10.6	–0.027	0	15.2	0.109	0.031	16.7	–0.278	0.044
	15:00 T _a	21.2	0.161	0.079	18.5	–0.004	0	29.4	–0.148	0.023	26.6	–0.17	0.092	30.5	–0.195	0.042
	15:00 T _d	11.5	0.166	0.096	7	0.086	0.016	11.3	–0.089	0.002	17.2	–0.087	0.02	18.1	–0.328	0.04
Fargo	Frequency	–	–	–	16.9	–0.389	0.021	6	–0.331	0.015	21.1	1.034	0.086	1	0.088	0.018
	3:00 T _a	15.2	0.203	0.179	10.3	0.222	0.181	18.2	0.094	0.008	18.8	0.108*	0.063*	23.2	0.118	0.018
	3:00 T _d	12.1	0.172	0.114	8	0.157	0.068	12.5	–0.048	0.001	16.1	0.077	0.022	18.6	0.321	0.061
	15:00 T _a	25	0.042	0.005	21.4	0.108*	0.046*	32.5	–0.132	0.027	28	–0.143	0.106	33.3	–0.07	0.005
	15:00 T _d	12.7	0.164	0.090	8.1	0.17	0.055	12.7	–0.035	0.001	17.6	0.031	0.003	19.9	–0.149	0.017

* Fargo's daily maximum DP temperatures increased with $p < 0.05$ significance, while DP temperatures at 15:00 did not. Conversely, Fargo's MT temperatures at 3:00 increased with $p < 0.05$ significance, while daily minimum MT temperatures did not. Statistical significance between daily and hourly datasets matched for all other trends.

Table 2

Summary statistics for paired urban and rural sites' trends in diurnal temperature range (°C) over 1948–2019 within the May 20–September 10 season. Linear regression slopes are expressed as decadal changes. Bold slope and R2 values indicate $p < 0.05$ significance.

	All			DP			DT			MT			MT+		
	Mean	Slope	R ²	Mean	Slope	R ²									
Minneapolis	11.1	-0.239	0.355	11.5	-0.255	0.156	14.2	-0.221	0.083	10.8	-0.206	0.367	11.2	-0.054	0.005
Jordan	12.5	-0.156	0.037	13.2	-0.29	0.077	15.3	-0.116	0.011	11.8	-0.108	0.025	11.9	0.002	0
Rochester	11.7	-0.288	0.352	12.5	-0.279	0.267	15.4	-0.041	0.003	11.2	-0.214	0.427	11.6	-0.061	0.014
Grand Meadow	11.9	-0.091	0.043	12.4	-0.194	0.094	13.8	0.085	0.009	11.3	0.008	0	11.9	-0.102	0.021
Duluth	11.7	-0.134	0.129	12.7	-0.244	0.242	15.8	-0.085	0.01	12.2	-0.301	0.308	12	-0.077	0.004
Two Harbors	11.4	-0.274	0.409	11.6	-0.243	0.207	16.1	-1.033	0.343	11.7	-0.606	0.350	13.9	-0.299	0.017
Fargo	13	-0.149	0.121	13.9	-0.063	0.018	16.7	-0.21	0.071	12.2	-0.193	0.231	13.4	-0.315	0.085
Ada	13.8	-0.28	0.248	14.3	-0.361	0.288	16.7	-0.418	0.193	13	-0.146	0.075	14.4	-0.34	0.076

3. Results

3.1. Observed SSC analysis of urban areas

3.1.1. Air mass frequency trends

All four urban sites experience both polar types and both moderate types throughout the year, with DP and MP peaking in winter and DM and MM peaking in summer (Fig. 1b). DT and MT are present from March to November, though to varying degrees. DT tends to peak in spring, though never exceeding 8% of any month's days. MT is far more common in all locations, especially in summer, with MT+ occurring most often in Minneapolis. Transition days occur about 10–15% of the time in each location throughout the year.

The frequency of MT days has significantly increased in all four cities, ranging from 1.0 additional days decade⁻¹ in Fargo to 1.8 days decade⁻¹ in Rochester (Table 1). In all cities except Rochester, the increase in MT has occurred along with a decrease in DP frequency. This is consistent with trends found in other studies in the Midwest (Knight et al., 2008; Vanos et al., 2014). TR frequency has roughly halved in all locations, aligning with a more geographically widespread downward trend (Kalkstein et al., 1998; Knight et al., 2008).

3.1.2. Air mass character trends

Diurnal temperature range has decreased in all locations (Table 2) as a result of increasing daily minimum air temperatures everywhere except Grand Meadow. It decreased more in southern urban sites (i.e., Minneapolis-St Paul and Rochester) than in their rural counterparts (i.e., Jordan and Grand Meadow), while it decreased more in northern rural sites (i.e., Ada and Two Harbors) than in their urban counterparts (i.e., Fargo-Moorhead and Duluth). Daily minimum air temperature has increased the most in Minneapolis, followed by the urban-rural pair of Duluth and Two Harbors, by 0.30, 0.28, and 0.24 °C 10 yr⁻¹, respectively. Daily maximum air temperatures show no statistically significant trends except for a 0.14 °C 10 yr⁻¹ increase in Duluth and a 0.18 °C 10 yr⁻¹ decrease in Ada (Table 1). Both the 3:00 and 15:00 dew point temperatures increased by 0.1 to 0.25 °C 10 yr⁻¹ in all urban locations, which is consistent with the increase in MT airmass frequency.

These urban trends do not occur uniformly over all air masses. MT afternoon temperatures actually decreased over the period of record, while nighttime temperatures increased in Minneapolis and Fargo by 0.17 and 0.11 °C 10 yr⁻¹. MT dewpoint temperatures increased in Rochester at both times, while only in Minneapolis at night. Other than a large decrease in afternoon dewpoint temperatures of -0.41 °C 10 yr⁻¹ in Rochester, there are no statistically significant trends in DT air or dewpoint temperatures. Nighttime air temperatures have increased in DP airmasses at all urban sites, and Rochester and Fargo have also had increases in dewpoint temperatures at both 3:00 and 15:00. MT+ air masses were too infrequent to show any statistically significant trends.

3.1.3. Consecutive day analysis

Because consecutive days of oppressive heat conditions exert a cumulative negative impact on health (Anderson and Bell, 2009; Hajat et al., 2006; Nairn and Fawcett, 2014), we quantified occurrences of three or more consecutive days under either DT (and DT+) or MT+ (and MT++) air masses at the four urban sites. We found no statistically significant trends in the frequency of these 3+ day episodes (Table 3), and at least half of the years included no such episodes at all. Duluth, where DT is especially rare and MT+ is virtually nonexistent, only had 11 DT/MT+ episodes over the entire period (1961 contained two episodes). Minneapolis experienced 61 episodes, including 15 years featuring at least two (1976 contained six episodes). Rochester and Fargo had 29 and 49 episodes, respectively. Minneapolis's episodes grew longer over the period, with annual mean duration increasing by 1.6 days over the 1948–2019 period (from 3.4 to 5.0 days per event), while Rochester's grew shorter by 2.3 days over the period. The longest recorded episodes in Minneapolis and Rochester lasted nine days each, occurring in 2012 and 1955, respectively. The longest episodes recorded at Fargo and Duluth occurred in May 1980 and lasted ten and five days, respectively.

3.1.4. Heatwave behaviors

As defined by the Excess Heat Factor (EHF) criteria, heatwaves show virtually no trends in frequency or characteristics at our sites (Table 4), and the length of the heatwave season was highly variable, with some years featuring only a single three-day heatwave or none at all, while the longest season lasted 131 days in Minneapolis and Rochester in 1959. Heatwaves lasted an average of 5.0 to 5.7 days and occurred an average of 3.5 to 4.0 times per year, totaling 20 to 22 days in an average season. The longest average heatwave ranged from 7.5 days in Fargo to 8.9 days in Rochester. Only two years in Duluth featured a heatwave lasting 15 days or more, and only three in Fargo; meanwhile, Minneapolis experienced six such years and Rochester experienced ten. Duluth shows an increasing trend in the number of heatwave days, adding 1.3 heatwave days 10 yr⁻¹ ($p < 0.1$).

Table 3

Summary statistics for urban sites' trends in frequency (occurrences per summer) and duration (days per occurrence) of consecutive runs of 3 or more MT+/DT days over 1948–2019 within the May 20–September 10 season. Linear regression slopes are expressed as decadal rather than yearly changes. Bold slope and R² values indicate $p < 0.05$ significance.

	Minneapolis			Rochester			Duluth			Fargo		
	Mean	Slope	R ²	Mean	Slope	R ²	Mean	Slope	R ²	Mean	Slope	R ²
Consecutive run frequency	0.8	0.027	0.002	0.4	0.013	0.001	0.2	0.001	0	0.7	-0.014	0.001
Consecutive run duration	4.2	0.221	0.128	4.2	-0.32	0.245	3.3	-0.117	0.143	3.6	-0.085	0.027

Table 4

Summary statistics for urban sites' trends in positive-EHF heat wave events over 1948–2019. T95 indicates the 95th-percentile temperature threshold (°C), while EHF85 indicates the 85th-percentile EHF value threshold (°C²). Frequency and duration are expressed as in Table 3.3. Heat wave season starting dates are expressed as Julian dates. Linear regression slopes are expressed as decadal changes. Bold slope and R2 values indicate p < 0.05 significance.

	Minneapolis			Rochester			Duluth			Fargo		
T ₉₅	25.8			24.2			21.7			24.7		
EHF ₈₅	17.8			15.7			17.4			18.1		
	Mean	Slope	R ²	Mean	Slope	R ²	Mean	Slope	R ²	Mean	Slope	R ²
Heatwave frequency	3.5	0.154	0.025	3.9	-0.063	0.004	3.7	0.132	0.019	4	-0.028	0.001
Heatwave duration, annual mean	5.8	-0.073	0.007	5.5	-0.14	0.032	5.4	0.074	0.009	5	-0.007	0
Heatwave duration, annual maximum	8.6	0.096	0.002	8.9	-0.37	0.027	7.8	0.423	0.062	7.5	-0.003	0
Heatwave season length	52.9	2.225	0.02	61.3	-0.773	0.002	48.8	2.948	0.044	56.4	1.407	0.011
Heatwave season starting date	174.2	-0.622	0.004	169.5	0.664	0.004	179.6	-1.244	0.016	176.4	-0.032	0
Exceedance of T ₉₅ on heatwave days	0.8	-0.029	0.016	0.8	-0.038	0.028	0.8	0.039	0.03	0.8	-0.037	0.031
Exceedance T ₉₅ on severe heatwave days	3.1	0.062	0.04	2.9	0.003	0	3.3	0.052	0.033	3.1	-0.013	0.001
Number of heatwave days	20.8	0.884	0.018	22	-0.896	0.02	19.9	1.316	0.049	20.7	0.037	0
Number of severe heatwave days	3.8	-0.083	0.002	4	-0.296	0.016	3.7	0.021	0	3.5	-0.225	0.016

Across all heatwave days in each location, MT was the most represented air mass, ranging from 37% of heatwave days in Fargo to 49% in Rochester (Table 5). DM was the second most represented in all cities except Minneapolis, where it came in a close third behind DT. TR days accounted for 7–10% of heatwave days in all four locations. Even MM, typically not a particularly warm type, covered 10% of heatwave days in Duluth, where the traditional oppressive MT+ and DT types were least frequent. For severe heatwave days only, MT+ and DT were better represented, covering 62% of such days in Minneapolis, roughly half of all severe heatwave days in Rochester and Fargo, and less than a quarter of them in Duluth, where nearly half were still MT.

3.2. Simulated SSC analysis of MSP region

A comparison of model-simulated SSC in the grid cell comprising the Minneapolis-St Paul (MSP) metropolitan region with SSC calculated from the MSP international airport historic record is provided in Supplementary Material (section S1). Simulated SSCs will not have any TR days as transitions are periods of rapid surface pressure change and surface pressure was not available in the model output; therefore, categories other than TR will be amplified in frequency in the model analysis. Even though air temperature in the Liess et al. dataset was bias-corrected, differences will occur between historic records and model output because of the coarseness of the model grid cell (i.e., 10 km) among other issues (e.g., errors in historic records, uncertainty in the dataset used for bias correction). These uncertainties propagate to the future projections, however, our aim in this study is to use the Liess et al. dataset as it is provided.

3.2.1. Air mass frequency trends

SSC calendars generated from the four simulated climate scenarios demonstrated a 21st-century shift toward more frequent tropical air mass types and less frequent polar types. DT had the greatest net gain in frequency under both RCP4.5 and RCP8.5, while DM had the greatest net loss (Table 6, Fig. 2). However, DM remained the most common summer air mass except under END8.5, where it was narrowly outnumbered by MT. Though overrepresented already in the historical simulations relative to the observed record, DT

Table 5

Allocation of daily SSC categories within all positive-EHF heat wave days and within severe heat wave days only. Values are expressed as total days over 1948–2019 and as percentages of each location's heat wave or severe heat wave day.

		DP	DM	DT	MP	MM	MT	MT+	TR
Minneapolis	All heatwave days	0	274	299	1	35	642	139	161
		(0.0%)	(17.7%)	(19.3%)	(0.1%)	(2.3%)	(41.4%)	(9.0%)	(10.4%)
	Severe heatwave days	0	16	105	0	0	70	73	24
		(0.0%)	(5.6%)	(36.5%)	(0.0%)	(0.0%)	(24.3%)	(25.3%)	(8.3%)
All heatwave days	1	310	229	0	67	786	73	139	
	(0.1%)	(19.3%)	(14.3%)	(0.0%)	(4.2%)	(49.0%)	(4.5%)	(8.7%)	
Rochester	Severe heatwave days	0	15	88	0	1	110	46	29
		(0.0%)	(5.2%)	(30.4%)	(0.0%)	(0.3%)	(38.1%)	(15.9%)	(10.0%)
	All heatwave days	12	501	109	4	148	554	25	110
		(0.8%)	(34.2%)	(7.5%)	(0.3%)	(10.1%)	(37.9%)	(1.7%)	(7.5%)
Duluth	Severe heatwave days	1	56	45	0	5	130	17	16
		(0.4%)	(20.7%)	(16.7%)	(0.0%)	(1.9%)	(48.1%)	(6.3%)	(5.9%)
	All heatwave days	5	376	302	1	35	558	70	156
		(0.3%)	(25.0%)	(20.1%)	(0.1%)	(2.3%)	(37.1%)	(4.7%)	(10.4%)
Severe heatwave days	0	22	97	0	1	70	42	22	
	(0.0%)	(8.7%)	(38.2%)	(0.0%)	(0.4%)	(27.6%)	(16.5%)	(8.7%)	

Table 6

Summary statistics for simulated air mass frequency (days per season), as well as frequency (occurrences per season) and duration (days per occurrence) of consecutive runs of 3 or more MT+/DT days. All statistics represent Minneapolis within the May 20–September 10 season over four climate scenarios. Air mass frequencies and consecutive run frequencies represent 160 observations, with one value per model-year combination. Consecutive run durations represent individual events unaggregated by model or year (number of observations = 160 × number of events per average model-year). Bold mean values indicate significant changes from HIST (p < 0.05 by t-test).

		HIST		MID		END4.5		END8.5	
		Mean	Std Dev	Mean	Std Dev	Mean	Std Dev	Mean	Std Dev
Air mass frequency	DP	5.3	5.7	3.8	3.8	2.5	2.3	1.2	1.6
	DM	40.9	14.2	40.7	12.8	34.5	11.6	28.7	10.6
	DT	13.0	12.8	17.6	14.1	21.0	16.0	26.9	20.4
	MP	11.2	7.3	7.2	5.7	7.5	5.0	5.9	4.6
	MM	22.2	16.5	14.8	8.7	18.5	13.5	16.5	11.1
	MT	20.4	9.2	27.7	11.6	26.4	11.0	29.5	11.5
	MT+	1.0	1.3	2.2	2.5	3.5	3.5	5.3	4.6
	Frequency	1.8	1.9	2.6	2.2	3.1	2.2	3.9	2.4
Consecutive runs	Duration	5.3	3.3	5.3	3.3	5.8	4.1	6.5	5.4

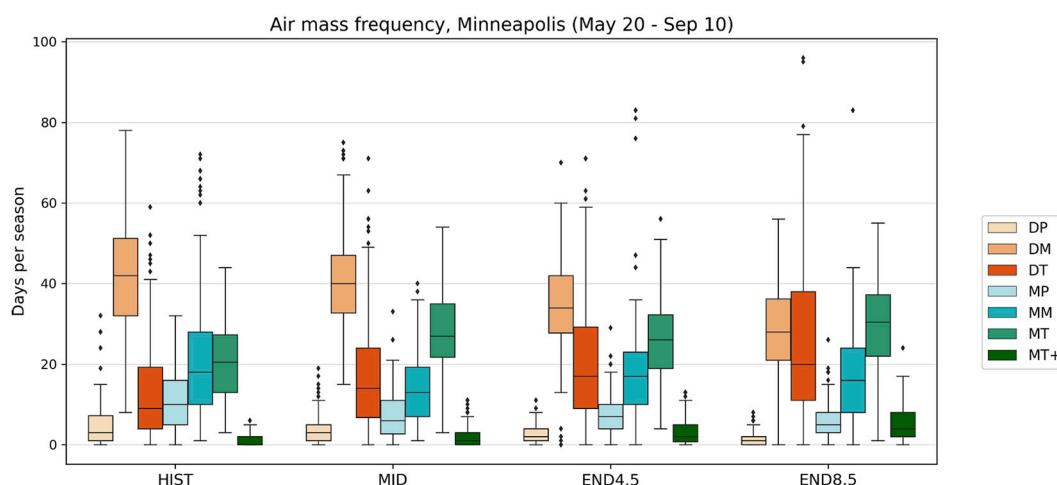


Fig. 2. Distributions of summer (May 20–September 10) air mass frequency by scenario. Whiskers indicate $1.5 \times$ IQR, with outlying values plotted individually. Each observation represents one model-year combination (see Table 6 for full description).

doubled in average frequency from HIST to END8.5, and increased by over 60% under END4.5. While falling short of exceeding MT frequency in summer in END8.5, DT showed much more year-to-year and intermodel variability in frequency, with the greatest standard deviation among model-years of any air mass in future simulations. DT’s frequency increases were proportional within the months in which it already occurred under HIST, with almost no expansion beyond the March–October range it already occupied (Fig. S3).

Under all scenarios, it continued to peak in frequency in July and August, which is later than observed historically, (Figs. S4-S6). Contrary to DT, DP days were already underrepresented in simulated historical summers and diminished further in frequency in future simulations. Most model runs nearly or even completely eliminated DP from July and August under the END8.5 scenario, while substantially weakening its presence throughout the rest of the year. MT and MT+ become more frequent in the future scenarios, MT increasing by 7 days by MID and END4.5 and continuing to increase 2 additional days by END8.5 (Table 6, Fig. 2). MT+ days increase from 1 per summer under HIST to over 5 by END8.5, while DP frequency decreases by about the same amount (Table 6). MT amplified its presence in summer, widening its seasonal distribution around a consistent June peak (Figs. S5-S6). Likewise, MT+ expanded into earlier spring, later summer, and fall while continuing to feature most prominently in April through June.

3.2.2. Air mass character trends

Each air mass type is projected to warm in future scenarios, mainly driven by increases in nighttime air temperatures along with increases in dewpoint temperatures (Table S2). As DT is projected to become a more frequent air mass over Minneapolis, the differences in relative risk of mortality between a hotter DT day and a cooler DT day may become increasingly relevant. More analysis is provided in Supplementary Material (section S2).

3.2.3. Consecutive day analysis

With increases in frequency of MT+ and DT days, there were corresponding increases in episodes of 3 or more consecutive oppressive days. All future scenarios featured a significant increase in episode frequency, more than doubling from HIST to END8.5 (Table 6, Fig. 3). This closely matches the approximate doubling of DT frequency between those same scenarios; DT days remained far more common than MT+ days in every scenario and therefore contributed to the bulk of these consecutive episodes. Tails of episode length distributions grew longer with time and under higher emissions (Fig. S14), but except under RCP8.5, changes in average episode length were minimal and statistically insignificant. Caution should be taken in projecting absolute number of episodes, given the model bias toward higher frequency of both MT+ and DT days, therefore an assumption is made that the change in number of episodes is realistic. Importantly, while the historical record at MSP shows no trend in frequency of heat episodes, these model simulations project a statistically significant increase in the future.

3.2.4. Heatwave behaviors

Temperature thresholds above which excess mortality becomes more likely vary by location-specific climatology (Curriero et al., 2002), but the transfer of this concept to the same location under a changed climate has proven challenging to address (Kinney et al., 2008). In our future climate scenarios, 95th percentiles of daily mean temperature demonstrated a clear increase, by as much as 4.6 °C by end-century under RCP8.5 (Table 7), however, the EHF method considers exceedances of this T_{95} value. Because of bias adjustment of the WRF dataset, the HIST average T_{95} compared well with that of Minneapolis station observations (within 0.5 °C; Table 4). However, the HIST average EHF₈₅ severity threshold was 4.6 °C² lower than that of observations, potentially indicating less intra-seasonal temperature variability. EHF₈₅ only increased in mid-century, instead decreasing slightly in both end-century scenarios. This corresponds with future severe heatwave days' exceedances of their own scenarios' respective T_{95} thresholds, which increased in MID and decreased in END8.5 (Table 7). Though this might suggest a lack of increased summer temperature variability in Minneapolis as its warming progresses, the EHF₈₅ threshold is not intended primarily as a climatological indicator of summer variability, but instead as a predictor of the conditions most likely to produce severe health outcomes.

Because the EHF quantifies extremes, these results suggest that while these cities are becoming hotter, variability around the T_{95} may increase by mid-century but will then decrease by the end of the century. EHF assumes that humans can acclimatize to environmental conditions and will be stressed if temperatures exceed this normal, which in this case is the T_{95} under each emissions scenario. Simulated future heatwave seasons maintained nearly identical starting dates and showed no statistically significant lengthening or shortening across scenarios (Table 7). This indicates that the hottest 5% of annual weather conditions can be expected to continue occupying the same overall time frame within summer rather than becoming biased earlier or later in the year. This consistency within the seasonal cycle across scenarios aligns with the consistency of monthly ranges in which hotter air masses, especially DT, are projected to occur (Figs. S3-S6), although at increasing frequencies within its monthly range. This study did not examine future allocations of air mass types on positive-EHF days, but as DT is projected to grow dramatically in frequency, it occurs more regularly in consecutive stretches, and expands its margin above MT+ as the hottest air mass type. It is expected to be particularly well-represented within heatwaves.

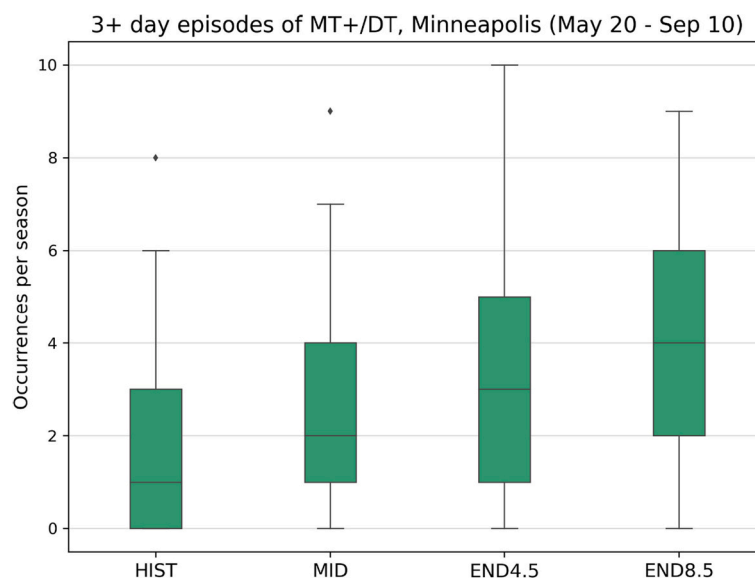


Fig. 3. Distributions of annual episode frequency of 3 or more consecutive MT+/DT days by scenario, within the May 20–September 10 season. Whiskers indicate $1.5 \times$ IQR, with outlying values plotted individually. Each observation represents one model-year combination (see Table 6 for full description).

Table 7

Summary statistics for simulated trends in positive-EHF heat wave events, defined from each model-scenario combination's simulated future T95 threshold. All statistics represent Minneapolis over four climate scenarios. T95 indicates the 95th-percentile temperature threshold (°C), while EHF85 indicates the 85th-percentile EHF value threshold (°C²); means and standard deviations for these summarize eight values, one from each model-scenario. Heat wave frequencies, heat wave season lengths, heat wave season starting dates (Julian date), number of heat wave days, and number of severe heat waves represent 160 observations, with one value per model-year combination. All other rows represent individual days or events unaggregated by model or year (number of observations = 160 × number of days or events per average model-year). Bold mean values indicate significant changes from HIST ($p < 0.05$ by t -test).

	HIST		MID		END4.5		END8.5	
	Mean	Std Dev	Mean	Std Dev	Mean	Std Dev	Mean	Std Dev
T ₉₅	26.3	1.1	28.2	1.5	29.0	1.3	30.9	2.2
EHF ₈₅	13.2	5.0	16.3	5.1	11.6	3.0	11.5	2.7
Heatwave frequency	3.3	1.9	3.5	1.7	3.1	1.6	3.0	1.5
Heatwave duration	6.6	5.1	6.1	4.1	6.9	5.5	7.0	5.8
Heatwave season length	47.2	29.3	51.5	28.7	45.1	28.7	42.3	27.5
Heatwave season starting date	178.2	20.6	176.5	23.1	176.7	20.8	178.7	18.7
Exceedance of T ₉₅ on heatwave days	0.9	1.8	1.0	2.0	0.9	1.6	0.9	1.6
Exceedance of T ₉₅ on severe heatwave days	2.8	1.8	3.1	1.7	2.6	1.4	2.5	1.4
Number of heatwave days	21.6	15.3	21.4	11.1	21.3	13.9	21.1	13.6
Number of severe heatwave days	3.8	4.9	3.8	4.2	3.9	4.4	4.0	4.0

4. Discussion and conclusions

Despite the large scale of synoptic air masses, Minnesota does not experience heat events equally. By some SSC and EHF-based evaluations, the southern cities of Minneapolis and Rochester are more prone to oppressive heat conditions than the northern cities of Fargo and Duluth. Under other measures, such as frequency and temperature characteristics of DT airmasses, Fargo more closely resembles the southern cities than Duluth. Fargo and Duluth share comparable latitudes, but DT and MT+ occur at Minneapolis-like frequencies in Fargo while remaining extremely rare in Duluth, likely due to the cooling from Lake Superior.

The widening of urban-rural distinctions over the historic record suggests a greater urban heat island influence than climate change influence, at least in the two southern urban-rural locations examined here, though the format of this study is insufficient to confirm this. Given the greater magnitude in future warming projected by Liess et al. (2022) in northern rather than southern Minnesota, it is possible that such patterns are already in effect, thus leaving the southern rural sites least affected by either warming influence. Meanwhile, the model-based portion of this study specifically addresses climate change, but does not account for thermal modifications of air masses at the urban or intra-urban scale, due to the spatial limitations of the WRF model outputs.

Air mass character distinctions among the four simulated climate scenarios suggest that the dry air mass categories can be expected to remain fairly dry until end-century, while the moist categories may become more humid sooner and, aside from MP, accrue little to no additional humidity between mid-century and end-century. Under moderate or high emissions, daytime temperatures in MT and MT+ are not projected to increase further beyond the levels reached by mid-century. Meanwhile, the bulk of their projected nighttime warming is expected to occur later in the century, especially under high emissions. This will result in a MT/MT+ diurnal temperature range that widens in mid-century and then narrows in end-century. Some of these results are unexpected, as narrower diurnal ranges frequently accompany increased humidity, but in this case the two effects do not show an intuitive temporal alignment. The balance of health impacts under greater humidity but minimally warmer nights on MT/MT+ days would need to be examined specifically for Minneapolis in order to determine what this implies for mid-century public health risks. Under both end-century scenarios, the combination of more humid MT/MT+ days and warmer MT/MT+ nights implies a heightened risk of mortality and morbidity. The difference between moderate and high emissions is more substantial for DT days, which are expected to become hotter by mid-century, then either stay roughly the same under moderate emissions or heat considerably further under high emissions by end-century.

The findings of this study suggest that while some changes in extreme heat conditions in Minnesota are already occurring, such as the increasing frequency of MT at the expense of DP and the pattern of nighttime warming, other projected trends represent new directions in Minnesota's climate not foreshadowed by the previous seven decades, such as the increased frequency and temperature of DT days. Because dry heat (DT) and humid heat (MT and MT+) produce different physiological responses among humans, and may raise different relative risks of mortality within distinct age demographics, these trends carry important implications for public health in Minnesota's urban areas. However, the increasing abundance of DT days raises the question of whether DT is likely to remain a useful indicator of health-threatening conditions, as does the increased variability in 15:00 temperatures among DT days under the high emissions scenario. If DT begins to rival MT in frequency, as is projected to occur in an average year under END8.5, then DT+ may begin to fulfill a similar role to that of MT+, delineating the most extreme subset of DT days from the larger DT pool, possibly too large to pose a consistent risk to health. Despite its own relative increases in frequency under all three future scenarios, MT+ will likely remain infrequent enough to maintain its status as a meaningful signifier of oppressively hot and humid days that more consistently constitute a public health concern. Just as MT days on the warmer or more humid end, which fall short of qualifying as MT+, may still be associated with above-baseline mortality, the same may be true for future DT days. This is especially relevant given the continued rarity of DT+ in all future scenarios, remaining much less common than MT+ even under END8.5.

Regardless of the magnitude of the heat-related risk facing each location, Minnesota's urban population centers will need to be

prepared to address the health concerns associated with the growing frequency, duration, and intensity of extreme heat events. Such preparations will need to draw from a thorough understanding of the unique sensitivities of each city population's health responses to heat. This can be accomplished through predictive algorithms (Hayhoe et al., 2010; Sheridan and Kalkstein, 2004) or other relative risk-based assessments (Curriero et al., 2002; Kalkstein et al., 2018), which can then be applied to future climate projections for an urban location (Sheridan et al., 2012). A critical component of local heat-health evaluations is the identification and quantification of disparities in health outcomes based on age, race, income, and other demographics. This can then facilitate more targeted “cool cities solutions” efforts toward specific neighborhoods or populations where vulnerabilities are greatest (de Guzman et al., 2020).

Minnesota has long been a leader in climate action planning, and to meet the Executive Order (19–37) to reduce statewide greenhouse gas emissions to levels at least 80% below 2005 levels by 2050 (<http://climate.state.mn.us>), communities are asking for high resolution climate projections to develop their mitigation and adaptation action plans. Future work will involve creating user-friendly interfaces for the dataset analyzed in this study (Liess et al., 2022) and updates to our projections with downscaled CMIP6 models for the urban-rural paired sites and state of Minnesota.

Funding

This work was supported by U.S. Department of Agriculture National Institute for Food and Agriculture, grant number 2019-67019-30463, and the Department of Soil, Water, and Climate Allmaras-Howe Fellowship, University of Minnesota.

Data availability

SSC data and corresponding climate projection data for MSP from this project can be found at the University of Minnesota Digital Conservancy system, <https://conservancy.umn.edu/drum>.

CRedit authorship contribution statement

Jonathan F.H. Birkel: Conceptualization, Methodology, Software, Validation, Formal analysis, Investigation, Data curation, Writing – original draft, Visualization. **Tracy E. Twine:** Conceptualization, Methodology, Resources, Writing – original draft, Supervision, Project administration, Funding acquisition. **Stefan Liess:** Methodology, Software, Investigation, Writing – review & editing. **Larry S. Kalkstein:** Conceptualization, Methodology, Writing – review & editing. **Scott Sheridan:** Methodology, Software, Investigation, Resources, Writing – review & editing.

Declaration of Competing Interest

The authors declare that they have no known competing financial interests or personal relationships that could have appeared to influence the work reported in this paper.

Appendix A. Supplementary data

Supplementary data to this article can be found online at <https://doi.org/10.1016/j.uclim.2022.101307>.

References

- Anderson, B.G., Bell, M.L., 2009. Weather-related mortality: How heat, cold, and heat waves affect mortality in the United States. *Epidemiology* 20 (2), 205–213.
- Bergeron, T., 1930. Richtlinien einer dynamischen klimatologie. *Meteorol. Z.* 47, 246–262.
- Curriero, F.C., Heiner, K.S., Samet, J.M., Zeger, S.L., Strug, L., Patz, J.A., 2002. Temperature and mortality in 11 cities of the eastern United States. *Am. J. Epidemiol.* 155 (1), 80–87. <https://doi.org/10.1093/aje/155.1.80>.
- Dahl, K., Licker, R., Abatzoglou, J.T., Delet-Barreto, J., 2019. Increased frequency of and population exposure to extreme heat index days in the United States during the 21st century. *Environ. Res. Commun.* 1 (7), 075002 <https://doi.org/10.1088/2515-7620/AB27CF>.
- Daly, C., Slater, M.E., Roberti, J.A., Laseter, S.H., Swift, L.W., 2017. High-resolution precipitation mapping in a mountainous watershed: ground truth for evaluating uncertainty in a national precipitation dataset. *Int. J. Climatol.* 37, 124–137. <https://doi.org/10.1002/joc.4986>.
- de Guzman, E., Kalkstein, L.S., Sailor, D., Eisenman, D., Sheridan, S., Kirner, K., et al., 2020. Rx for Hot Cities: Climate Resilience through Urban Greening and Cooling in Los Angeles. TreePeople and Los Angeles Urban Cooling Collaborative. Retrieved from. <https://www.treepeople.org/wp-content/uploads/2020/09/RX-for-hot-cities-report.pdf>.
- Fischer, E.M., Oleson, K.W., Lawrence, D.M., 2012. Contrasting urban and rural heat stress responses to climate change. *Geophys. Res. Lett.* 39 (3) <https://doi.org/10.1029/2011GL050576>.
- Folkerts, M.A., Bröde, P., Botzen, W.J.W., Martinius, M.L., Gerrett, N., Harmsen, C.N., Daanen, H.A.M., 2020. Long term adaptation to heat stress: shifts in the minimum mortality temperature in the Netherlands. *Front. Physiol.* 11 <https://doi.org/10.3389/fphys.2020.00225>.
- Founda, D., Santamouris, M., 2017. Synergies between urban Heat Island and heat waves in Athens (Greece), during an extremely hot summer (2012). *Sci. Rep.* 7 (1) <https://doi.org/10.1038/s41598-017-11407-6>.
- Habeeb, D., Vargo, J., Stone, B., 2015. Rising heat wave trends in large US cities. *Nat. Hazards* 76 (3), 1651–1665. <https://doi.org/10.1007/s11069-014-1563-z>.
- Hajat, S., Armstrong, B., Baccini, M., Biggeri, A., Bisanti, L., Russo, A., et al., 2006. Impact of high temperatures on mortality: is there an added heat wave effect? *Epidemiology* 17 (6), 632–638. <https://doi.org/10.1097/01.ede.0000239688.70829.63>.

- Harlan, S.L., Brazel, A.J., Prashad, L., Stefanov, W.L., Larsen, L., 2006. Neighborhood microclimates and vulnerability to heat stress. *Soc. Sci. Med.* 63 (11), 2847–2863. <https://doi.org/10.1016/j.socscimed.2006.07.030>.
- Hayhoe, K., Sheridan, S., Kalkstein, L., Greene, S., 2010. Climate change, heat waves, and mortality projections for Chicago. *J. Great Lakes Res.* 36 (Suppl. 2), 65–73. <https://doi.org/10.1016/j.jglr.2009.12.009>.
- Hondula, D.M., Vanos, J.K., Gosling, S.N., 2014. The SSC: a decade of climate-health research and future directions. *Int. J. Biometeorol.* 58 (2), 109–120. <https://doi.org/10.1007/s00484-012-0619-6>.
- Kalkstein, L.S., Davis, R.E., 1989. Weather and human mortality: an evaluation of demographic and interregional responses in the United States. *Ann. Assoc. Am. Geogr.* 79 (1), 44–64. <https://doi.org/10.1111/j.1467-8306.1989.tb00249.x>.
- Kalkstein, L.S., Greene, J.S., 1997. An evaluation of climate/mortality relationships in large U.S. cities and the possible impacts of a climate change. *Environ. Health Perspect.* 105 (1), 84–93. <https://doi.org/10.1289/ehp.9710584>.
- Kalkstein, L.S., Sheridan, S.C., Graybeal, D.Y., 1998. A determination of character and frequency changes in air masses using a spatial synoptic classification. *Int. J. Climatol.* 18 (11), 1223–1236. [https://doi.org/10.1002/\(SICI\)1097-0088\(199809\)18:11<1223::AID-JOC310>3.0.CO;2-1](https://doi.org/10.1002/(SICI)1097-0088(199809)18:11<1223::AID-JOC310>3.0.CO;2-1).
- Kalkstein, L.S., Greene, S., Mills, D.M., Samenow, J., 2011. An evaluation of the progress in reducing heat-related human mortality in major U.S. cities. *Nat. Hazards* 56 (1), 113–129. <https://doi.org/10.1007/s11069-010-9552-3>.
- Kalkstein, A.J., Kalkstein, L.S., Vanos, J.K., Eisenman, D.P., Grady Dixon, P., 2018. Heat/mortality sensitivities in Los Angeles during winter: a unique phenomenon in the United States. *Environ. Health A Glob. Access Sci. Source* 17 (1), 45. <https://doi.org/10.1186/s12940-018-0389-7>.
- Kinney, P.L., O'Neill, M.S., Bell, M.L., Schwartz, J., 2008. Approaches for estimating effects of climate change on heat-related deaths: challenges and opportunities. *Environ. Sci. Pol.* 11 (1), 87–96. <https://doi.org/10.1016/J.ENVSCL.2007.08.001>.
- Knight, D.B., Davis, R.E., Sheridan, S.C., Hondula, D.M., Sitka, L.J., Deaton, M., et al., 2008. Increasing frequencies of warm and humid air masses over the conterminous United States from 1948 to 2005. *Geophys. Res. Lett.* 35 (10) <https://doi.org/10.1029/2008GL033697>.
- Lau, N.C., Nath, M.J., 2012. A model study of heat waves over North America: meteorological aspects and projections for the twenty-first century. *J. Clim.* 25 (14), 4761–4764. <https://doi.org/10.1175/JCLI-D-11-00575.1>.
- Lee, W.V., 2013. Historical global analysis of occurrences and human casualty of extreme temperature events (ETEs). *Nat. Hazards* 70 (2), 1453–1505. <https://doi.org/10.1007/S11069-013-0884-7>.
- Liess, S., Twine, T.E., Snyder, P.K., Hutchison, W.D., Konar-Steenberg, G., Keeler, B.L., Brauman, K.A., 2022. High-resolution climate projections over Minnesota for the 21st century. *Earth Space Sci.*, e2021EA001893 <https://doi.org/10.1029/2021EA001893>.
- Loridan, T., Coates, L., Frontiers, R., Argüeso, D., Perkins-Kirkpatrick, S.E., 2016. The excess heat factor as a metric for heat-related fatalities: defining heatwave risk categories (no. 4). *Austral. J. Emergency Manag.* 31, 31–37.
- Luber, G., McGeehin, M., 2008, November. Climate change and extreme heat events. *Am. J. Prevent. Med. Elsevier*. <https://doi.org/10.1016/j.amepre.2008.08.021>.
- Meehl, G.A., Tebaldi, C., 2004. More intense, more frequent, and longer lasting heat waves in the 21st century. *Science* 305 (5686), 994–997. <https://doi.org/10.1126/science.1098704>.
- Nairn, J.R., Fawcett, R.J.B., 2014. The excess heat factor: a metric for heatwave intensity and its use in classifying heatwave severity. *Int. J. Environ. Res. Public Health* 12 (1), 227–253. <https://doi.org/10.3390/ijerph120100227>.
- Nairn, J.R., Ostendorf, B., Bi, P., 2018. Performance of excess heat factor severity as a global heatwave health impact index. *Int. J. Environ. Res. Public Health* 15 (11). <https://doi.org/10.3390/ijerph15112494>.
- Scalley, B.D., Spicer, T., Jian, L., Xiao, J., Nairn, J., Robertson, A., Weeramanthri, T., 2015. Responding to heatwave intensity: excess heat factor is a superior predictor of health service utilisation and a trigger for heatwave plans. *Aust. N. Z. J. Public Health* 39 (6), 582–587. <https://doi.org/10.1111/1753-6405.12421>.
- Semenza, J.C., McCullough, J.E., Flanders, W.D., McGeehin, M.A., Lumpkin, J.R., 1999. Excess hospital admissions during the July 1995 heat wave in Chicago. *Am. J. Prev. Med.* 16 (4), 269–277. [https://doi.org/10.1016/S0749-3797\(99\)00025-2](https://doi.org/10.1016/S0749-3797(99)00025-2).
- Sheridan, S.C., 2002. The redevelopment of a weather-type classification scheme for North America. *Int. J. Climatol.* 22 (1), 51–68. <https://doi.org/10.1002/joc.709>.
- Sheridan, S.C., Dixon, P.G., 2017. Spatiotemporal trends in human vulnerability and adaptation to heat across the United States. *Anthropocene* 20, 61–73. <https://doi.org/10.1016/j.ancene.2016.10.001>.
- Sheridan, S.C., Kalkstein, L.S., 2004. Progress in heat watch-warning system technology. *Bull. Am. Meteorol. Soc.* 85 (12), 1931–1941. <https://doi.org/10.1175/BAMS-85-12-1931>.
- Sheridan, S.C., Kalkstein, A.J., Kalkstein, L.S., 2009. Trends in heat-related mortality in the United States, 1975–2004. *Nat. Hazards* 50 (1), 145–160. <https://doi.org/10.1007/s11069-008-9327-2>.
- Sheridan, S.C., Lee, C.C., Allen, M.J., Kalkstein, L.S., 2012. Future heat vulnerability in California, part I: projecting future weather types and heat events. *Clim. Chang.* 115 (2), 291–309. <https://doi.org/10.1007/s10584-012-0436-2>.
- Smoliak, B.V., Snyder, P.K., Twine, T.E., Mykleby, P.M., Hertel, W.F., 2015. Dense network observations of the twin cities canopy-layer urban Heat Island*. *J. Appl. Meteorol. Climatol.* 54 (9), 1899–1917. <https://doi.org/10.1175/JAMC-D-14-0239.1>.
- Vanos, J.K., Kalkstein, L.S., Sanford, T.J., 2014. Detecting synoptic warming trends across the US Midwest and implications to human health and heat-related mortality. *Int. J. Climatol.* <https://doi.org/10.1002/joc.3964>.
- Vicedo-Cabrera, A.M., Scovronick, N., Sera, F., Royé, D., Schneider, R., Tobias, A., et al., 2021. The burden of heat-related mortality attributable to recent human-induced climate change. *Nat. Clim. Chang.* 11 (6), 492–500. <https://doi.org/10.1038/s41558-021-01058-x>.
- Vose, R.S., Easterling, D.R., Kunkel, K.E., LeGrande, A.N., Wehner, M.F., 2017. Temperature changes in the United States. In: Wuebbles, D.J., Fahey, D.W., Hibbard, K. A., Dokken, D.J., Steward, B.C., Maycock, T.K. (Eds.), *Climate Science Special Report: Fourth National Climate Assessment, Volume 1*. U. S. Global Change Research Program, Washington, DC, USA, pp. 185–206. <https://doi.org/10.7930/JON29V45>.
- Watts, J.D., Kalkstein, L.S., 2004. The development of a warm-weather relative stress index for environmental applications. *J. Appl. Meteorol.* 43 (3), 503–513. [https://doi.org/10.1175/1520-0450\(2004\)043<0503:TDOAWR>2.0.CO;2](https://doi.org/10.1175/1520-0450(2004)043<0503:TDOAWR>2.0.CO;2).